J Supercond Nov Magn (2011) 24: 549–557
DOI 10.1007/s10948-010-0999-y

ORIGINAL PAPER

Inorganic Magnetite Precipitation at 25 °C: A Low-Cost Inorganic Coprecipitation Method

T. Perez-Gonzalez · A. Rodriguez-Navarro · C. Jimenez-Lopez

Received: 11 September 2010 / Accepted: 15 September 2010 / Published online: 15 October 2010

Abstract An easy, low-cost coprecipitation method to inorganically produce magnetite nanoparticles from solutions, in free-drift experiments, under anoxic conditions, at 25 °C and 1 atm pressure is here presented. By using this method, pure magnetite is obtained as the final solid, which shows the typical magnetic properties and thermal stability behavior of magnetite produced by other methods. The size of the magnetite crystals produced by the present method varies from relatively big sizes (200–300 nm), to sizes within the single magnetic domain range, just depending on the incubation time. The solution from which magnetite precipitates may be representative of certain natural environments where bacteria that produce magnetite may live and, thus, our magnetite may be used as an inorganic reference to compare to biologically produced magnetites.

Keywords Magnetite · Coprecipitation · Biomarker · Mineral synthesis · Magnetitc nanoparticles

1 Introduction

Magnetite is a ferrous-diferric iron oxide (Fe_3O_4). It is a magnetic mineral that is usually found in magmatic, metamorphic and sedimentary rocks ([1] and references therein). It is also an important part of terrestrial and marine sediments [2, 3], degradated oil deposits [4], estuarian and lake sediments [5, 6] and it is even found in extraterrestrial materials like Martian meteorite ALH84001 [1]. Because magnetite can be precipitated inorganically and by organisms, this mineral is currently used as a biomarker to recognize biotic/abiotic origin of natural magnetites found in terrestrial and extraterrestrial environments. Prokaryotes (bacteria) biomineralize magnetite through two methods that differ mechanistically, the so-called biologically induced mineralization (BIM) and biologically controlled mineralization (BCM) [7, 8]. While magnetite nanocrystals produced by BIM are known to be synthesized by the dissimilatory iron-reducing bacteria and are deposited external to the cell, BCM magnetites are synthesized by the magnetotactic bacteria, and some higher organisms and are precipitated intracellularly, and in the case of bacteria, as membrane-bounded structures called magnetosomes. These magnetites have unique crystal morphologies and a narrow size range, leading to their original use as magnetofossils. The problem, however, is the lack of inorganic magnetite formed under environmental conditions similar to those where microorganisms that produce magnetite live, that can be used as an inorganic reference material to compare biotic samples with.

Moreover, because of its strong magnetic properties, magnetite has important applications in nanotechnology, ranging from magnetic storage [9], magnetic ink printing [10], magnetic refrigeration, photoelectric devices and ferrofluids [11], magnetic bioseparation [12], and microwave absorption [13], among others, to clinical applications such as cancer therapy [14], tumor detection [15], magnetic resonance imaging for clinical diagnosis contrast agents [16] and magnetic drug targeting [14]. Other applications of the magnetic nanoparticles are: in-vitro cell separation [17], in-vivo drug delivery [18], immunoassay [19], immunomagnetic array [20], enzyme immobilization [21] and biosensors and bioprocessing [22, 23]. Because of these applications, the

T. Perez-Gonzalez · C. Jimenez-Lopez (✉)
Departamento de Microbiología, Facultad de Ciencias, Universidad de Granada, Campus de Fuentenueva s/n, 18071, Granada, Spain
e-mail: cjl@ugr.es

A. Rodriguez-Navarro
Departamento de Mineralogía, Universidad de Granada, Campus de Fuentenueva s/n, 18071, Granada, Spain

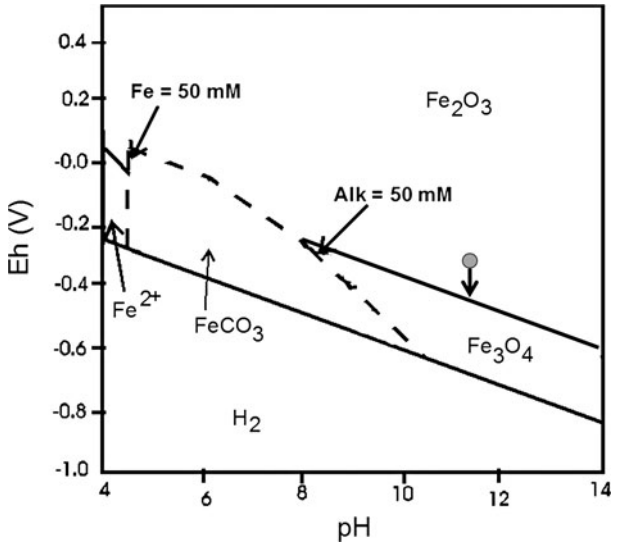

Fig. 1 Stability diagram for magnetite (Fe_3O_4) and siderite ($FeCO_3$) in a closed system. A *grey dot* represents initial conditions after titration. *Arrow* indicates the possible displacement of the initial solution during the course of time of the experiment. Since Fe^{3+} is initially removed to form Fe^{3+} oxides, the Eh decreases, thus approaching (or entering) the stability field for magnetite

production of magnetite represents one of the most promising fields of applied nanotechnology and is a rapidly growing business that generates millions of dollars.

This mineral can be synthesized in the laboratory as a primary or secondary phase. The best-developed techniques for the synthesis of inorganic magnetite as a primary mineral phase are based on magnetite precipitation from bulk solution. There are a number of different specific methods to do this, some of which are detailed below, which mainly differ in how Fe^{2+} is introduced in the solution. All these methods, however, are dependent on controlling the conditions consistent with the thermodynamic stability field for magnetite, which include Eh, pH and alkalinity/pCO_2, as shown in Fig. 1.

Most of the procedures involving the precipitation of magnetite from bulk solution follow the so-called "coprecipitation" method, in which a variety of salts of Fe^{2+} and Fe^{3+} mixtures (mainly as chlorides or nitrates) are introduced as starting solutions under anaerobic conditions. In order to maintain the conditions necessary for the thermodynamic stability field for magnetite, different compounds are used to increase and maintain alkaline conditions during magnetite precipitation including the following: NH_3 at 85 °C [24, 25], NaOH at 25 °C in agarose gel [26], NaOH at 25–45 °C in solution [24], NH_3 and/or NaOH at 9–90 °C [27]. NH_4OH at 25 °C [28], and $N(CH_3)_4OH$ [24]. It is common for the magnetite crystals formed in this manner to have several different morphologies (within the same reaction mixture) including cubic, rounded, octahedral and/or irregular. For those applications in which specific sizes and relatively narrow size distributions of the magnetite particles are desired, several modifications of the bulk "coprecipitation" technique have been developed. These modifications are mainly based on limiting the space available for crystal growth by precipitating magnetite in microemulsions, vesicles, polymer solutions, or gels [29–31].

Other methods for the inorganic precipitation of magnetite are the "reduction-precipitation" technique, in which the precipitation of magnetite occurs by the addition of iron only as a Fe^{3+} solution (mainly $FeCl_3$), and the subsequent reduction of this cation by different means, and the "electrochemical" method, in which a constant voltage is applied to the solution to obtain and maintain the necessary Eh value range to comply with the stability field for magnetite. Magnetite can also be precipitated at high temperatures, which results in the synthesis of larger, morphologically well-defined crystals. One example is the formation of magnetite by the oxidation of Fe^{2+} solutions at 90 °C by the addition of KNO_3 [32] and the mixing of solutions of $FeSO_4 \cdot 7H_2O$ and $N_2H_4 \cdot H_2O$ and the subsequent heating of the reaction mixture in an autoclave at 150 °C for 8 hours [33]. However, methods involving high-temperature magnetite precipitation are expensive when extrapolated to industrial production for technological applications. Therefore, low-cost methods to produce inorganic magnetite could be further developed avoiding high temperatures and maintaining the system at room temperature.

Also, most of the abovementioned methods are mainly designed to cover specific technological application, and, therefore, the precipitation of magnetite occurs in an environment that does not usually represent natural conditions. In this scenario, the problem arises when it comes to compare inorganic magnetite to biotic magnetite. Therefore, the aim of this paper is to design a method to precipitate magnetite at room temperature, under conditions that are compatible with life and, simultaneously, under conditions that can be found in natural environments. To comply with these objectives, the precipitation of magnetites has been performed at 25 °C, from free-drift experiments, by following a coprecipitation method in which magnetite formed from a solution containing carbonate salts, which are commonly found in natural environments. This study proposes an easy method to precipitate inorganic magnetite, which is compatible with natural environments. The resulting magnetite has been extensively characterized and it is a good candidate to be used as an inorganic reference to compare to biotic magnetite.

2 Materials and Methods

2.1 Materials

All chemicals used $NaHCO_3$, Na_2CO_3, $FeCl_3$, $Fe(ClO_4)_2$ and NaOH were of reagent grade from Sigma Aldrich.

O_2-free deionized water (Milli-Q) was prepared by boiling deionized water for one hour, and then cooling in an ice bath while sparging with ultra pure N_2 for one hour. Once cold, the oxygen-free water is immediately placed inside an anaerobic Coy chamber.

2.2 Experimental Procedures

Experiments were carried out inside an anaerobic chamber (Coy Lab) at room temperature and 1 atm pressure. The atmosphere inside the chamber was N_2/H_2 (4%) mixture. The trace O_2 inside the chamber was removed by two palladium pellets, which catalyze the reaction of such oxygen with the hydrogen that fills the chamber to form water. Silica gel was also introduced inside the Coy chamber to remove the excess of H_2O and keep the humidity level below 30%. The chamber was also equipped with gas analyzers to continually monitor $O_{2(g)}$ and $H_{2(g)}$ levels throughout the course of the experiment.

To initiate the experiments, a $NaHCO_3/Na_2CO_3$ solution (0.75 L, 25 mM/25 mM) was prepared using MilliQ water. It was boiled, bubbled with CO_2 during an hour and placed quickly into the Coy chamber to keep it anaerobic. $Fe(ClO_4)_2$ was added to this solution up to a 25 mM concentration. This solution with the following composition: 25 mM $NaHCO_3$, 25 mM $NaCO_3$ and 25 mM $Fe(ClO_4)_2$ with a pH value of 7.79 and a Eh value of −392 mV is here referred as initial solution.

With the goal of driving the initial solution into the calculated stability field of magnetite (i.e. high pH values and low Eh values), different volumes of solutions of NaOH (1 M) and $FeCl_3$ (0.5 M) were added to the initial solution while the Eh and pH values were monitored continuously. The solutions of $FeCl_3$ and NaOH were prepared by mixing the reactives with O_2-free water. A volume of 100 ml of NaOH and 26 ml of $FeCl_3$ were added to the initial solution to reach a pH value of 11.68 and an Eh value of −301.7 mV (Table 1). This solution, with a final concentration of 22.2 mM of $NaHCO_3$, 22.2 mM of $NaCO_3$, 22.2 mM of $Fe(ClO_4)_2$, 11.5 mM of $FeCl_3$ and 89 mM of NaOH is here referred to as MIS solution. This MIS solution was poured in three 1 L Pyrex bottles until they were completely filled. The Pyrex bottles were tightly closed with Teflon caps and kept at 25 °C inside the Coy chamber for a month (here referred to as MIS30). With the goal of determining the effect of the incubation time on the size of magnetite, other sets of experiments were performed identically to those explained above, but they were incubated just for four days (here referred as MIS 4).

Table 1 Values of the pH, Eh and $Fe^{2+}_{(aq)}$ at the beginning, after titration, and at the end of each of the MIS4 and MIS30 experiments

Experiment type	pH ±0.05	Eh (mV) ±13 mV	$Fe^{2+}_{(aq)}$ (mM) ±0.1
Initial solution	7.79	−392	4.1
MIS (0 days)	11.68	−301.7	0.123
MIS (4 days)	11.74	−300.2	0.119
MIS (30 days)	11.82	−290.2	0.101

2.3 Analysis

A volume of 20 ml of the master solutions was saved for chemical analyses (dissolved O_2, $Fe^{2+}_{(aq)}$ and $Fe_{T(aq)}$). The dissolved O_2 was measured on 10 ml of the master solution by using the K-7759 CHEMets kit. Accuracy was ±10 ppm. The pH and Eh values were measured by using a portable Thermo Orion 250 A+ pH meter, calibrated using NIST-traceable standard buffer solutions for slope correction (pH 4 and 7) and temperature compensation, while the calibration for Eh measurements was performed by using quinhydrone added to the standard buffer solutions at pH 4 and 7, according to the manufacturer's instructions. Based on repeated measurements, the accuracy for pH and Eh was calculated as ±0.05 and ±13 mV (1σ), respectively. Aqueous ferrous cation ($Fe^{2+}_{(aq)}$) and total iron ($Fe_{T(aq)}$) were measured by using the 1,10-Phenanthroline method for Fe^{2+} and the Ferrover method for the $Fe_{T(aq)}$ (Hach, manufacturer's instructions) with a Hach DR 850 colorimeter. The analytical error for both analyses was ±1 μM. $Fe^{3+}_{(aq)}$ concentration was calculated as the difference between the measured values of $Fe_{T(aq)}$ iron and $Fe^{2+}_{(aq)}$.

After the complexion of the experiments (4 days and 30 days), the solutions were filtered under vacuum through a 0.45 μm Millipore membrane within the anaerobic chamber to avoid potential oxidation of the solid samples. The solutions were chemically analyzed as detailed above. The filtered solids were immediately freeze-dried (FLEXI-DRY-μP).

The mineralogy of the solids, collected in both MIS30 and MIS4 experiments, was determined by using a single-crystal x-ray diffractometer equipped with an area detector (Bruker D8 SMART APEX, Germany). A frame (or 2D diffraction pattern) was collected using the following experimental conditions: Mo Kα, 50 kV, 30 mA, 0.5 mm collimator diameter and 30 seconds exposure time. Sample powders, agglutinated by using glue, were analyzed in transmission mode. XRD2DScan software [34] was used to convert 2D diffraction patterns into regular 2θ linear scans. This software was also used for background subtraction and integration of peaks in the 2θ scans.

The morphology and size of the crystals collected in MIS30 and MIS4 experiments were studied by Transmission Electron Microscopy (TEM). The microscope used was

a Philips CM20, equipped with Energy Dispersive x-ray Microanalysis (EDAX). These analyses allowed the study of the morphology of the solids, the d-spacing [determined from selected area electron diffraction (SAED)] and the gross chemical composition of individual crystals. For TEM analyses, samples were fixed with glutaraldehyde. Afterward, the sample was dehydrated with ethanol, and embedded in Embed 812 resin. Ultrathin sections (50–70 nm) were prepared (Reicher Ultracut S microtome, DIATOME diamond blade). The samples were placed in copper grids and carbon coated.

The magnetic susceptibility, hysteresis loop and first magnetization curve were determined on 2.490 mg of the MIS30 solid, by using a MANICS DSM-8 magnetometer, at 300 and 10000 Mg.

Differential scanning calorimetry analyses (DSC) were performed on 9.608 mg of MIS30 samples by using a SHIMADZU model TGA-50H thermogravimeter. The samples were analyzed under anaerobic conditions to avoid potential oxidations. The heating rate was 10 °C min^{-1}. Thermogravimetric analysis (TGA) was also run on ≈10 mg of solid, by heating the sample in an alumina cell under N_2 atmosphere, at a rate of 20 °C min^{-1} up to a final temperature of 950 °C. The gases evolved during the decomposition of the solid were, as well, analyzed.

Raman analyses (Kaiser HoloSpec, with a He–Ne 632.8 nm laser interfaced with a Nikon Eclipse E600 microscope) were run on ≈1 mg of MIS30 sample. Spectra were collected over a 100–3800 cm^{-1} range at a spectral resolution of 4 cm^{-1}. Since the samples were highly thermolabile, a very low laser power (0.4 mW) and a long acquisition time (3 min) was used. Nevertheless, the spectra showed a very low intensity and a small noise to signal ratio. Spectra were taken at several different points from each sample to check their consistency.

3 Results and Discussion

The solution, initially orange and non-magnetic, started to turn darker in a few minutes after titration and, two hours later, a black, strong magnetic precipitate was observed in the solution. Since Fe^{3+} oxide minerals are highly insoluble [32, 35] they will easily precipitate during the first stages of the process. Actually, this result is in accordance with that predicted by the Eh-pH diagram calculated for our experiments. As can be seen in Fig. 1, the MIS solution was slightly over the stability field for magnetite, situated in the stability field for Fe^{3+} oxides. Based on the Nernst equation, the Eh is described as follows:

$$Eh = E_0 + \frac{RT}{nF} \log \frac{Fe^{3+}}{Fe^{2+}} \tag{1}$$

where E_0 is the standard potential, R is the constant for the ideal gases, T is the temperature, n the numbers of electron accepted and F the Faraday constant. For the reaction of the oxidation of Fe^{3+}, at 25 °C, and assuming $\gamma_{Fe^{3+}}$ (activity coefficient for Fe^{3+}) and $\gamma_{Fe^{2+}}$ (activity coefficient for Fe^{2+}) equal to one, the Nernst equation could be written as follows [36]:

$$Eh = 0.77 + \frac{0.05916}{n} \log \left[\frac{Fe^{3+}}{Fe^{2+}} \right] \tag{2}$$

From this equation, once the Fe^{3+} oxides form in our MIS solution, the concentration of Fe^{3+} decreases, and so does the Eh value (Fig. 1). Since the pH is held constant, the MIS solution will eventually enter the stability field for magnetite, making the precipitation of such a mineral phase thermodynamically stable compared to that of the precipitation of Fe^{3+} oxides. Those previously formed Fe^{3+} minerals dissolve over the course of time of the experiment, the final solid being composed of 100% magnetite (octahedral isometric system), according to XRD analyses. The dissolution of previously formed mineral phases giving rise to more stable ones, described by the Ostwald Step Rule, is a well-known phenomenon observed to occur during the formation of minerals [37–40].

Regarding the morphology of the crystals, and according to TEM analyses, MIS4 samples are isomorphic (Figs. 2a and b), while MIS30 are rectangles, rhombuses, hexagons, bars and spherulites (Figs. 2c and d). Since these images are bi-dimensional cuts of three-dimensional crystals, the 3D morphology of the crystals cannot be determined exactly. Nevertheless, the 2D images corresponding to MIS30 sample can result from euhedric, prismatic, prismatic elongated in one direction, cubic and rhombic 3D crystals. The magnetite crystals from MIS4 experiments exhibit a size range from 40 to 50 nm (within the single magnetic domain range [41]), while the size of those from the MIS30 experiments is within the interval 300–400 nm (multimagnetic domain [41]). EDAX analyses of several crystals showed that the chemical composition of those crystals was Fe and O (Fig. 2d). SAED analyses of the crystals showed d-spacings consistent with magnetite.

It is remarkable that we have observed sizes of our inorganically produced magnetites that are much bigger than those obtained from other authors. It is also interesting that the size of our crystals could be modified just varying the time for the incubation, so the longer the incubation time, the bigger the crystals. Regarding coprecipitation methods, Nyirő-Kósa et al., [27] precipitated magnetite from solutions based on chloride salts, added with NH_4 and NaOH, at temperatures ranging from 9 to 90 °C. These authors obtained magnetite crystals within a size range from 11 to 120 nm, depending on the pH values (from 3.8 to 13.1). As in our experiments, these authors also observed varying morphologies associated to the size of the crystals. For instance, crystals with diameters between 10 and 25 nm had ir-

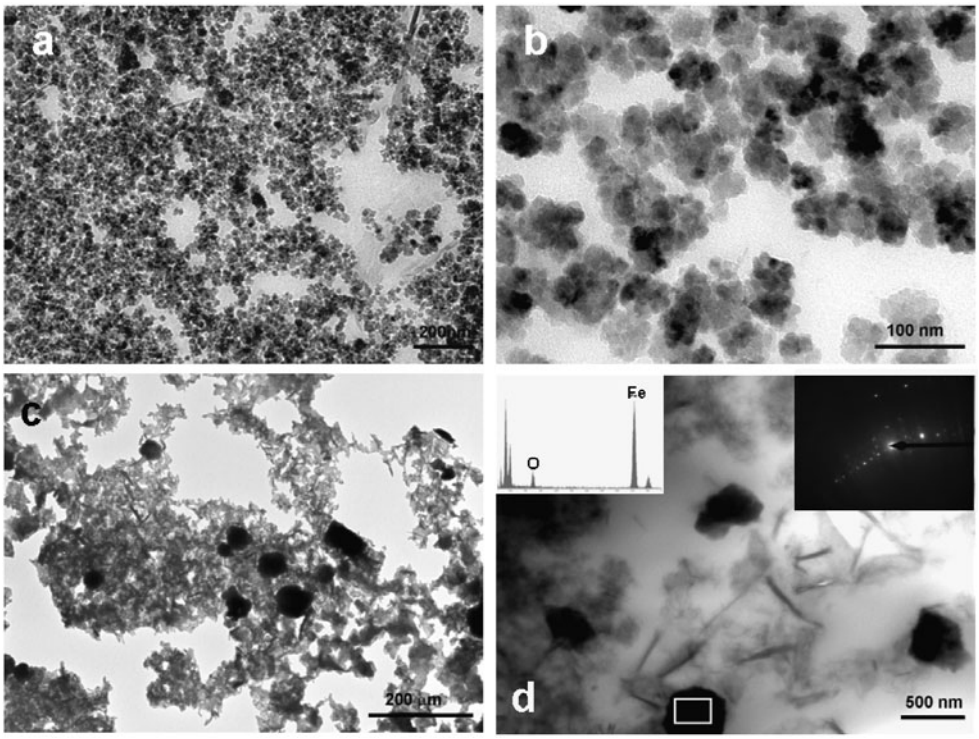

Fig. 2 TEM images and EDAX analyses of magnetite. (**a**) General image of MIS4 crystals. (**b**) Detail of MIS4 crystals. (**c**) General image of MIS30 crystals. (**d**) Detail of MIS30 crystals with SAED and EDAX analyses. The *white rectangles* on crystals show where EDAX and SAED analyses were performed

regular or rounded crystal morphologies, whereas those with diameters greater than 50 nm were octahedral. Vayssières et al. [24], also working with nitrate salts and $FeCl_2$ added with $NaNO_3$, NH_4NO_3 or $N(CH_3)_4NO_3$ obtained magnetite crystals, at a temperature range from 25 to 45 °C, with crystal sizes within the range from 1.5 to 12.5 nm, just depending on the pH values and ionic strength of the solution from which magnetite precipitated. The magnetites produced by a reduction-precipitation method are also usually small, with an average diameter of about 10 nm or even less [42, 43] and magnetites produced by electrochemical synthesis usually exhibit size ranges of 45–80 nm [44]. Interestingly, the size range of our magnetites is closer to that of the magnetites produced at high temperatures. For instance, the magnetites produced by Schwertmann and Cornell [32] by the oxidation of a Fe^{2+} solution ($FeSO_4$) at 90 °C had a size range of 0.05–0.20 μm. Also, Zhu et al. [33] obtained magnetite crystals of about 1 μm in diameter by mixing solutions of $FeSO_4 \cdot 7H_2O$ and $N_2H_4 \cdot H_2O$ and heating them at 150 °C for 8 hours. The fact that we are able to change the size based on the incubation time is probably due to the dissolution of the smaller crystal to favor the growth of the bigger ones, according to Ostwald ripening process [37]. By means of this process, the system reduces its free energy. Therefore, we propose an easy and low-cost method to inorganically produce magnetite at 25 °C, in which the magnetite crystals can exhibit relatively big sizes (200–300 nm), or sizes within the single magnetic domain range, just depending on the incubation time.

Moreover, the solution from which magnetite precipitate can be found in high-pH areas of natural environments where magnetite forms. For instance, Zachara et al. [45] and Perez-Gonzalez et al. [46] demonstrated that the precipitation of magnetite induced by *Shewanella oneidensis* requires high pH values for the precipitation to occur. Those high pH values are reached at the cell wall and decrease from this wall to the bulk culture medium, triggering the precipitation of magnetite precisely at the cell wall [45]. Therefore, although the pH values of the environment where bacteria grow is about 7 to 8, high pH values are locally created by bacterial metabolic activity in the surroundings of the cell wall, and this local environment may be represented by the solution from which our inorganic magnetite forms.

Much attention has been paid to determine whether or not the final solid was maghemite or magnetite. Most of the methods proposed so far in the relevant literature that claim to produce magnetite actually do not test whether the final product is indeed magnetite or maghemite. The differentiation between these two minerals phases is somewhat difficult just from XRD analyses, since only the reflections (221) and (320) [present in maghemite, but not in magnetite [47]] can distinguish both minerals. These reflections were not observed in the XRD pattern from our sample. Nevertheless, the distinction of these two minerals can be satisfactorily done by means of Raman analyses [48]. The spectrum shows a sharp peak at 670 cm^{-1} (Fig. 5), which is indicative for magnetite and also, for the good crystallinity of our sample (a poorly ordered substance would show a broader peak).

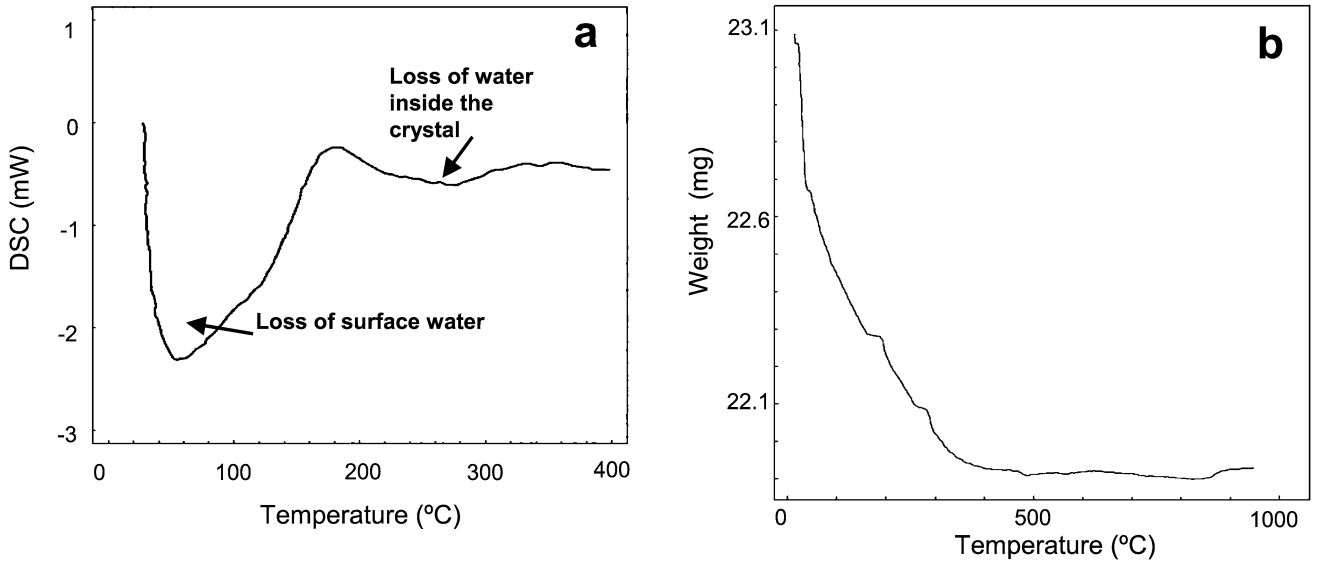

Fig. 3 (**a**) Differential scanning calorimetry (DSC) of the MIS30 sample. (**b**) Thermogravimetric analysis of the MIS30 sample. Mass loss is indicated in the figure

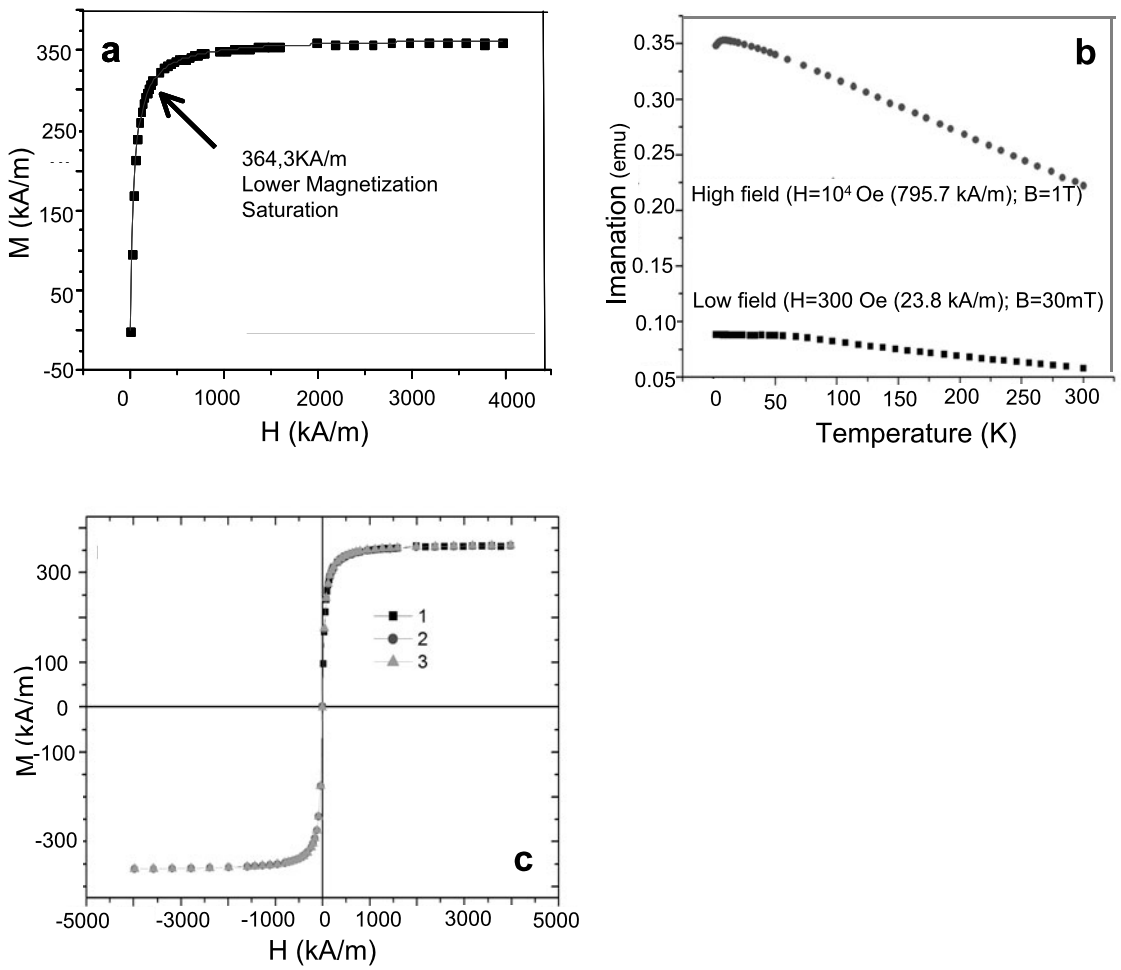

Fig. 4 Magnetic susceptibility curves for the MIS30 magnetite. (**a**) First imanation curve. (**b**) Different field imanation curves. (**c**) Hysteresis loop. *Squares* represent first field intensity which increases up to saturation point. *Dots* represent reduction of the field intensity up to negative values and saturation point. *Triangles* represent remagnetization because of the application of a positive field

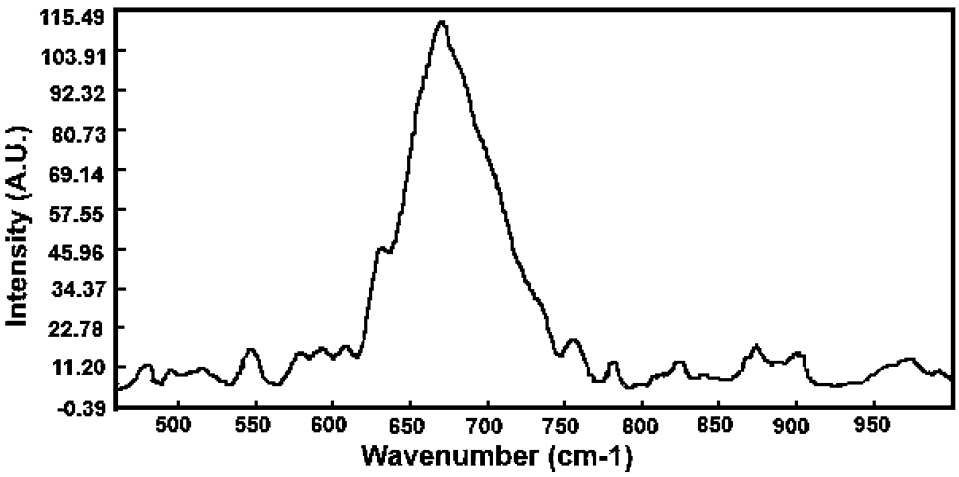

Fig. 5 Raman spectra of MIS30 magnetites

The characteristic peaks for maghemite (350, 512, 664, 726 and 1330 cm^{-1}) were not observed.

Chemical stability and the hydratation levels of the sample were analyzed by DSC (Fig. 3a). The sample shows two endothermic reactions, one at about 70°C and the second one within the interval 200–350°C. Both endothermic reactions correspond to two events of water loss. The first one, at lower temperatures, indicates a surface water loss, while the second reaction, at higher temperature, is associated to the loss of water inside the crystal. These two dehydration events are confirmed by TGA analyses of the magnetite (Fig. 3b). These analyses show a first mass lost within the 100–300°C range (the sample loses about 5% of its initial mass). Later, within the 300–400°C range, the sample underwent an additional 1% mass reduction. Analysis of evolved gases associated to both events indicated the only presence of H_2O.

Magnetic measurements of MIS30 magnetites show typical values for magnetite in both the first imanation curve and different field imanation curves (Figs. 4a and 4b). The lower magnetization saturation value determined for our sample (364.3 KA/m; Fig. 4a) is lower than the expected standard value for magnetite (570 KA/m). Such a difference is usual when the sample is hydrated [49]. The hydration of our sample is confirmed by TGA results, explaining the lower magnetization saturation value. However, the hysteresis loop (Fig. 4c) perfectly fits that of a soft magnetic material easy to magnetize and demagnetize, that curve being typically from magnetite [32].

4 Conclusions

We have developed an easy, low-cost method to inorganically produce magnetite under anaerobic conditions at 25°C in free-drift experiment. Within a time frame of days, 100% magnetite is produced with a varying size from the single magnetic domain range to the superparamagnetic range, just by controlling the time of incubation.

Moreover, the method proposed in this study is compatible with certain natural systems and the inorganic magnetite produced may be a good candidate as an inorganic reference to compare biogenic magnetites to.

Acknowledgements Financial funding was provided by grant CGL2007-63859 from the Spanish Ministry of Culture (MEC). ARN thanks to projects CTM2007-65713 from MEC and P08-RNM-4169 from junta de Andalucía. Thanks to Prof. Rull for Raman analysis, Prof. Delgado for helping in the interpretation of magnetic properties, Prof. Gonzalez-Muñoz for ideas and support, Prof. Romanek for providing the Coy chamber and to the CIC personal from the University of Granada for technical assistance.

References

1. Thomas-Keprta, K.L., Bazylinski, D.A., Kirschvink, J.L., Clemett, S.J., McKay, D.S., Wentworth, S.J., Vali, H., Gibson, E.K. Jr., Romanek, C.S.: Elongated prismatic magnetite crystals in ALH84001 carbonate globules: potential Martian magnetofossils. Geochim. Cosmochim. Acta **64**, 4049–4081 (2000). doi: 10.1016/S0016-7037(00)00481-6
2. Mozley, P.S., Carothers, W.W.: Elemental and isotopic composition of siderite in the Kupanuk Formation, Alaska: Effect of microbial activity and water/sediment interaction on early pore-water chemistry. J. Sediment. Petrol. **64**, 681–692 (1992)
3. Ptacek, C.J.: Experimental determination of siderite solubility in high ionic-strength aqueous solutions. Ph.D. Thesis, Univ. Waterloo, Waterloo, Ontario, Canada (1992)
4. Rajan, S., Mackenzie, F.T., Glenn, C.R.: A thermodynamic model for water column precipitation of siderite in the Plio-Pleistocene Black Sea. Am. J. Sci. **296**, 506–548 (1996)
5. Kelts, K.: Environments of deposition of lacustrine petroleum source rocks: an introduction. In Fleet, A.J., Kelts, K., Talbot, M.R. (eds.) Lacustrine Petroleum Source Rocks, vol. 40, pp. 3–26. Geol. Soc. Spec. Publ., London (1988)
6. Michard, A., Beucaire, C., Michard, G.: Uranium and rare earth elements in CO_2-rich waters from Vals-les Bains (France). Geochim. Cosmochim. Acta **51**, 901–909 (1988)

7. Frankel, R.B., Bazylinski, D.A.: Biologically induced mineralization by bacteria. Rev. Mineral. Geochem. **54**, 217–247 (2003). doi:10.2113/0540095
8. Bazylinski, D.A., Frankel, R.B.: Biologically controlled mineralization in prokaryotes. Rev. Mineral. Geochem. **54**, 95–114 (2003). doi:10.2113/0540217
9. Chakraborty, A.J.: Kinetics of the reduction of hematite to magnetite near its Curie transition. Magn. Magn. Mater. **204**, 57–60 (1999)
10. Peikov, V.T., Jeon, K.S., Lane, A.M.: Characterization of magnetic inks by measurements of frequency dependence of AC susceptibility. J. Magn. Magn. Mater. **193**, 307–310 (1999)
11. McMichael, R.D., Shull, L.J., Swartzendruber, L.H., Bennett, R.E., Walson, J.: Magnetocaloric effect in superparamagnets. Magn. Magn. Mater. **111**, 29–33 (1992)
12. Sen, T., Sebastianelli, A., Bruce, I.J.: Mesoporous silica-magnetite nanocomposite: Fabrication and applications in magnetic bioseparations. J. Am. Chem. Soc. **128**, 7130–7131 (2006)
13. Pinho, M.S., Gregori, M.L., Nunes, R.C.R., Soares, B.G.: Aging effect on the reflectivity measurements of polychloroprene matrices containing carbon black and carbonyl-iron powder. Polym. Degrad. Stab. **73**(1), 1–5 (2001)
14. Kim, D.K., Zhang, Y., Kehr, J., Klason, T., Bjelke, B., Muhammed, M.: Synthesis and characterization of surfactant-coated superparamagnetic monodispersed iron oxide nanoparticles. J. Magn. Magn. Mater. **225**(1–2), 256–261 (2001)
15. Kumagai, M., Kano, M.R., Morishita, Y., Ota, M., Imai, Y., Nishiyama, N., Sekino, M., Ueno, S., Miyazono, K., Kataoka, K.: Enhanced magnetic resonance imaging of experimental pancreatic tumor in vivo by block copolymer-coated magnetite nanoparticles with TGF-β inhibitor. J. Control. Release **140**(3), 306–311 (2009)
16. Wunderbaldinger, P., Josephson, L., Weissleder, R.: Tat peptide directs enhanced clearance and hepatic permeability of magnetic nanoparticles. Bioconjug. Chem. **13**, 264–268 (2002)
17. Begg, A.C., Sprong, D., Balm, A., Martin, J.M.C.: Premature chromosome condensation and cell separation studies in biopsies from head and neck tumors for radiosensitivity prediction. Radiother. Oncol. **62**, 335–343 (2002)
18. Roulin, V.G., Deverre, J.R., Lemaire, L., Hindré, F., Julienne, M.C.V., Vienet, R., Benoit, J.P.: Anti-cancer drug diffusion within living rat brain tissue: An experimental study using [3H](6)-5-fluorouracil-loaded PLGA microspheres. Eur. J. Pharm. Biopharm. **53**, 293–299 (2002)
19. Mura, C.V., Becker, M.I., Orellana, A., Wolff, D.J.: Immunopurification of Golgi vesicles by magnetic sorting. Immunol. Methods **260**, 263–271 (2002)
20. Call, D.R., Brockman, F.J., Chandler, D.P.: Detecting and genotyping *Escherichia coli* O157:H7 Using multiplexed PCR and nucleic acid microarrays. Int. J. Food Microbiol. **67**, 71–80 (2001)
21. Kanno, S., Oshima, K., Shimomura, M., Miyauchi, S.: Immobilization of enzyme to magnetic particles modified with polyacrylic acid. Polym. Prepr. **54**(1), 2385 (2005)
22. Perez, J.M., Simeone, F.J., Saeki, Y., Josephson, L., Weissleder, R.: Viral-induced self-assembly of magnetic nanoparticles allows the detection of viral particles in biological media. J. Am. Chem. Soc. **125**, 10192–10193 (2003)
23. Nixon, L., Koval, C.A., Noble, R.D., Slaff, G.S.: Preparation and characterization of novel magnetite-coated ion-exchange particles. Chem. Mater. **4**, 117–121 (1992)
24. Vayssières, L., Chanèac, C., Tronc, E., Jolivet, J.P.: Size tailoring of magnetite particles formed by aqueous precipitation: an example of thermodynamic stability of nanometric oxide particles. J. Colloid Interface Sci. **205**, 205–212 (1998). doi:10.1006/jcis.1998.5614
25. Tseng, J.Y., Chang, C.Y., Chen, Y.H., Chang, C.F., Chiang, P.C.: Synthesis of micro-size magnetic polymer adsorbent and its application for the removal of Cu(II) ion. Colloid Surf. A **295**, 209–216 (2007)
26. Prozorov, T., Mallapragada, S.K., Narasimhan, B., Wang, L., Palo, P., Nilsen-Hamilton, M., Williams, T.J., Bazylinski, D.A., Prozorov, R., Canfield, P.C.: Protein-mediated synthesis of uniform superparamagnetic magnetite nanocrystals. Adv. Funct. Mater. **17**, 951–957 (2007)
27. Nyirö-Kósa, I., Csákberényinagy, D., Pósfai, M.: Size and shape control of precipitated magnetite nanoparticles. Eur. J. Mineral. **21**, 293–302 (2009)
28. Arató, B., Szányi, Z., Flies, C., Schüler, D., Frankel, R.B., Buseck, P.R., Pósfai, M.: Crystal-size and shape distributions of magnetite from uncultured magnetotactic bacteria as a potential biomarker. Am. Mineral. **90**, 1233–1241 (2005). doi:10.2138/am.2005.1778
29. Mann, S., Hannington, J.P.: Formation of iron oxides in unilamellar vesicles. J. Colloid Interface Sci. **122**, 326–335 (1988). doi:10.1016/0021-9797(88)90368-2
30. Ward, A.J.I., Friberg, S.: Preparing narrow size distribution particles from amphiphilic association structure. MRS Bull. **14**, 41 (1989)
31. Liu, Z.L., Wang, X., Yao, K.L., Du, G.H., Lu, Q.H., Ding, Z.H., Tao, J., Ning, Q., Luo, X.P., Tian, D.Y., Xi, D.: Synthesis of magnetite nanoparticles in W/O microemulsion. J. Mater. Sci. **39**, 2633–2636 (2004). doi:10.1023/B:JMSC.0000020046.68106.22
32. Schwertmann, U., Cornell, R.M.: Iron Oxides in the Laboratory: Preparation and Characterization, 2nd edn. Wiley-VCH, Weinheim (2000)
33. Zhu, H., Yang, D., Zhu, L.: Hydrothermal growth and characterization of magnetite (Fe_3O_4) thin films. Surf. Coat. Technol. **201**, 5870–5874 (2007)
34. Rodriguez-Navarro, A.: XRD2DScan: new software for polycrystalline materials characterization using two-dimensional X-ray diffraction. J. Appl. Crystallogr. **39**, 905–909 (2006)
35. Schwertmann, U.: Solubility and dissolution of iron oxides. Plant Soil **130**(1–2), 1–25 (1991)
36. Garrels, R.M., Christ, C.L.: Solutions, Minerals and Equilibria, p. 450. Jones and Bartlett, Boston (1990)
37. Morse, J.W., Casey, W.H.: Ostwald processes and mineral paragenesis in sediments. Am. J. Sci. **288**, 537–560 (1988)
38. Ogino, T., Suzuki, T., Sawada, K.: The formation and transformation mechanism of calcium carbonate in water. Geochim. Cosmochim. Acta **51**, 2757–2767 (1987)
39. Jimenez-Lopez, C., Caballero, E., Huertas, F.J., Romanek, C.S.: Chemical, mineralogical and isotope behaviour, and phase transformation. Geochim. Cosmochim. Acta **65**(19), 3219–3231 (2001)
40. Jimenez-Lopez, C., Romanek, C.S., Huertas, F.J., Ohmoto, H., Caballero, E.: Oxygen isotope fractionation in synthetic magnesian calcite. Geochim. Cosmochim. Acta **68**(16), 3367–3377 (2004)
41. Butler, R.F., Banerjee, S.K.: Theoretical single-domain grain size range in magnetite and titanomagnetite. J. Geophys. Res. **80**, 4049–4058 (1975)
42. Schwertmann, U., Murad, E.: The influence of aluminum on iron oxides: XIV. Aluminum substituted magnetite synthesized at ambient temperatures. Clay Miner. **38**, 196–202 (1990). doi:10.1346/CCMN.1990.0380211
43. Qu, S., Yang, H., Ren, D., Kan, S., Zou, G., Li, D., Li, M.: Magnetite nanoparticles prepared by precipitation from partially reduced ferric chloride aqueous solutions. J. Colloid Interf. Sci. **215**, 190–192 (1999). doi:10.1006/jcis.1999.6185
44. Franger, S., Berthet, P., Berthon, J.: Electrochemical synthesis of Fe3O4 nanoparticles in alkaline aqueous solutions containing complexing agents. J. Solid State Eletrochem. **8**, 218–223 (2004)
45. Zachara, J.M., Kukkadapu, R.K., Fredrickson, J.K., Gorby, Y.A., Smith, S.C.: Biomineralization of poorly crystalline Fe(III) oxides by dissimilatory metal reducing bacteria (DMRB). Geomicrobiol. J. **19**, 179–207 (2002). doi:10.1080/01490450252864271

46. Perez-Gonzalez, T., Jimenez-Lopez, C., Neal, A.L., Rull-Perez, F., Rodriguez-Navarro, A., Fernandez-Vivas, A., Iañez-Pareja, E.: Magnetite biomineralization induced by *Shewanella oneidensis*. Geochim. Cosmochim. Acta **74**(3), 967–979 (2010)
47. Bernal, J.D., Dasgupta, D.R., Mackay, A.L.: Oriented transformations in iron oxides and hydroxides. Nature **28**, 654–647 (1957)
48. Hanesch, M.: Raman spectroscopy of iron oxides and (oxy)hydroxides at low laser power and possible applications in environmental magnetic studies. Geophys. J. Int. **177**, 941–948 (2009)
49. Lima, E., Brand, A.L., Arelaro, A.D., Goya, G.F.: Spin disorder and magnetic anisotropy in Fe_3O_4 nanoparticles. J. Appl. Phys. **99**(8), 083908 (2006)